

Selective Determination of Elastomer Distribution in Multicomponent Systems Using Proton-Detected ^{13}C Imaging

A. Spyros, N. Chandrakumar, M. Heidenreich, and R. Kimmich*

Universität Ulm, Sektion Kernresonanzspektroskopie, Albert-Einstein-Allee 11, 89069 Ulm, Germany

Received October 15, 1997; Revised Manuscript Received February 2, 1998

ABSTRACT: The application of the cyclic J cross-polarization (CYCLCROP) NMR imaging pulse sequence for the acquisition of proton-detected ^{13}C NMR images of elastomeric materials is described. In CYCLCROP a series of two polarization transfers in the sense $^1\text{H} \rightarrow ^{13}\text{C} \rightarrow ^1\text{H}$ is applied before imaging in order to select a specific ^1H nucleus J -coupled to a ^{13}C nucleus and filter out all other ^1H coherences. It is shown that in multicomponent systems this technique can be used to acquire selective images of one of the components by suitable selection of the cross-polarization transfer pair of CH_N nuclei. An important advantage of CYCLCROP imaging turns out to be its selectivity even in the case of completely unresolved ^1H lines, as they are often encountered in polymer proton spectra. By selecting the CH methine proton of PI for the cross-polarization transfer filter, we successfully recorded edited ^1H images of commercial natural abundance *cis*-polyisoprene, na-PI, in the presence of a second elastomeric material, whose ^1H coherences were completely edited out. With ^{13}C -enriched polyisoprene, ^{13}C -PI, synthesized in the laboratory, CYCLCROP was employed to record images of the spatial distribution of PI in mixtures of PI with polybutadiene, PB, and poly(hydroxyoctanoate), PHO. Two different mixing sequences for performing the cyclic J cross-polarization, MOIST and PRAWN, were examined. 2D NMR coherence transfer spectra of the single and the cyclic polarization transfer in the rotating frame are reported for PI in solution and in bulk. It is shown that the short effective relaxation time in the rotating frame, $T_{\rho,\text{eff}}$, reduces the efficiency of CYCLCROP compared to theoretical predictions. However, an at least 8-fold reduction in the experimental time required for the acquisition of images with the same S/N is obtained by using CYCLCROP instead of directly detected one-pulse ^{13}C NMR imaging.

Introduction

Magnetic resonance imaging (MRI) has been routinely used as an *in vivo* medical diagnostic tool during the past few years.¹ At the same time, the potential of this technique in addressing problems in a wide area of different fields, such as materials science, polymers, petrochemicals, or plants and agriculture has been realized.² A number of different techniques, such as magic echoes,³ multiple pulse line narrowing,⁴ magic angle spinning (MAS),⁵ and stray field imaging,⁶ developed to allow imaging experiments in solid polymers, have been recently reviewed. These techniques are necessary because of the large line widths inherent in the NMR spectra of these materials. In contrast, elastomers permit the application of conventional liquid-state imaging techniques due to their reduced static line width resulting from a combination of increased segmental mobility and reduced crystallinity. A number of studies have appeared in the literature dealing with a wide range of applications of NMR imaging in elastomers, including phase separation,⁷ aging^{7–9} and biodegradation,¹⁰ water uptake,^{11,12} morphology and defects,¹³ filler¹⁴ and cross-link¹⁵ distribution, and stress-induced effects.^{16–18}

Due to the 10 times wider relative chemical-shift range of ^{13}C , the transition from ^1H to ^{13}C NMR spectroscopy has proven to be a very significant step in polymer NMR research. Nevertheless, the application of direct ^{13}C imaging or localized spectroscopy in polymer science has been so far scarcely exploited.^{16,19–23} The main reason for this is the unfavorable magnetic properties of the ^{13}C nucleus, that is its low gyromagnetic ratio apart from a natural abundance of only 1.1%.

A number of techniques for the detection of ^{13}C nuclei via the protons coupled to them have been proposed in order to overcome this sensitivity problem. Indirect ^{13}C detection methods of this sort in principle provide the sensitivity of proton NMR by assuming the same number of nuclei.^{23–29} In the following, we refer to the cyclic cross-polarization (CYCLCROP) scheme^{24,28–30} with the pathway $^1\text{H} \rightarrow ^{13}\text{C} \rightarrow ^1\text{H}$. This method turned out to be particularly easy to implement and to be robust against artifacts. The variety of its applications have recently been demonstrated in studies of sugar metabolism in plants.³¹

With CYCLCROP indirect ^{13}C imaging, both initial excitation and detection are performed in the ^1H channel, thus increasing substantially the sensitivity of the experiment compared to that of one-pulse ^{13}C detection. Since the ^1H longitudinal relaxation times of a given CH_N group are usually shorter than the ^{13}C ones, the repetition time of the experiment can be kept shorter, allowing more transients to be accumulated in a given time. By suitable adjustment of the carrier frequencies of the spin-lock and contact pulses, the Hartmann–Hahn condition can be made selective so as to be satisfied only by a single pair of ^1H and ^{13}C J -coupled nuclei. Thus with the CYCLCROP technique one is able to record proton-detected ^{13}C images of a specific CH_N group, using the cyclic J cross-polarization sequence as a chemical shift selective isotopomer filter that rejects all unwanted proton coherences. A review comparing indirect ^{13}C mapping and spectroscopic ^1H imaging methods for the visualization of hydrocarbon distribution in materials has been recently published.³²

The advantages of applying the CYCLCROP imaging sequence to various problems related to polymer science, and especially to elastomers, are several. The majority

* To whom correspondence should be addressed.

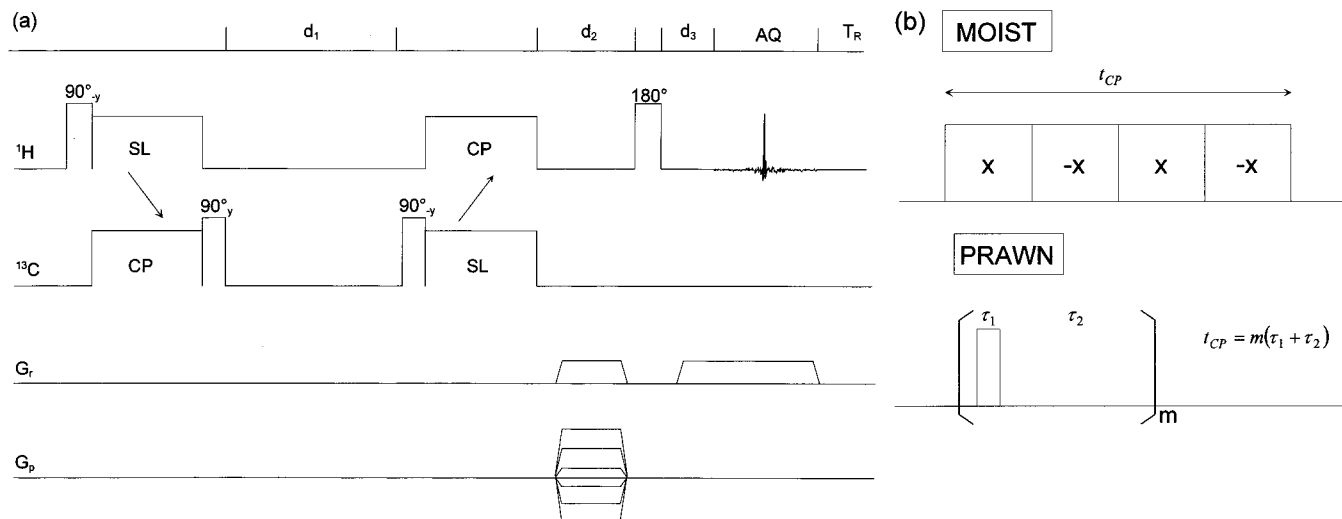
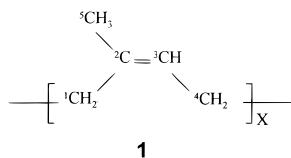


Figure 1. (a) CYCLCROP pulse sequence used for the acquisition of ^{13}C -edited ^1H NMR images. G_r and G_p are the read and phase gradients respectively, AQ is the acquisition interval, T_R is the recycle delay, d_1 is the ^1H spoil delay, and d_2 and d_3 are delays used to adjust the echo position. (b) MOIST and PRAWN methods of effecting cyclic cross-polarization. The cross-polarization time for PRAWN is given by $t_{CP} = m(\tau_1 + \tau_2)$.

of polymeric products used in everyday applications are heterogeneous materials, either blends of different polymers or mixtures of polymer and additives such as fillers, cross-linking agents, antioxidants, etc. An NMR imaging technique that can selectively probe the spatial distribution of one component out of a heterogeneous polymer material could provide important information regarding material inhomogeneities, phase separation, aging, and various structure–property relationships critical to performance. For this reason we decided to explore the utilization of the CYCLCROP sequence in obtaining proton-detected ^{13}C images of elastomeric materials. Two different variants to achieve polarization transfer were used. The first is based on the MOIST phase alternation scheme where the spin-lock (SL) and contact pulse (CP) interval is divided into segments of opposite phase.³³ The PRAWN variant permits robust operation with low average B_1 field amplitudes of the order of the coupling constant, employing a windowed comb of low flip angle contact and spin-lock pulses of fixed phase.³⁴

The NMR imaging experiments we will report were performed with two types of polyisoprene, **1** (PI), a commercial natural abundance *cis*-1,4 material, na-PI,



and *cis*-1,4-polyisoprene ^{13}C enriched at the methylene C-4 position, which was synthesized in the laboratory (^{13}C -PI). The advantages of CYCLCROP compared to direct ^{13}C detection imaging will be demonstrated. In addition, several factors that affect the efficiency of this NMR imaging technique when applied to elastomeric materials will be examined critically, so as to optimize future applications to more advanced problems in elastomer research. The differences of the MOIST and PRAWN cross-polarization variants of CYCLCROP imaging with respect to contrast formation in elastomers will also be examined.

Experimental Section

Natural abundance *cis*-polyisoprene was a gift from Dr. Sautter, Universität Ulm, and originated from Shell AG, Eschborn, IR 307. It had a weight average molecular weight M_w of 7.9×10^5 and a polydispersity index M_w/M_n of 1.7, as determined by GPC using polyisoprene standards of narrow M_w distribution. Its *cis*-percentage was determined as 80% by ^{13}C NMR spectroscopy. Polybutadiene, M_w 400 000, was purchased from Polysciences Inc., and its composition was specified as *cis*/*trans*/vinyl 36/55/9. Poly(hydroxyoctanoate), PHO, was a gift from Prof. R. H. Marchessault, McGill University. [$4\text{-}^{13}\text{C}$]Isoprene was synthesized by the Wittig reaction of $^{13}\text{CH}_3\text{Ph}_3\text{P}^+\text{I}^-$ with methacrolein in DMSO solvent. *cis*-1,4-Polyisoprene- $4\text{-}^{13}\text{C}$ was polymerized according to the procedure described in ref 35. The enrichment was 54% at the C-4 position (by ^1H NMR spectroscopy). ^1H NMR spectroscopic data in CDCl_3 solution are $\delta = 5.08$ ppm (b, 1H, methine H), 2.01 ppm (d, 2H, H-4, $J = 127$ Hz), 1.99 ppm (b, 2H, H-1), 1.63 ppm (s, 3H, methyl H). The microstructure of the ^{13}C -enriched PI polymer was determined by ^{13}C NMR spectroscopy as 79% *cis*, 15% *trans*, and 4.5% 3–4. The polymer had $M_w = 8500$ and $M_w/M_n = 3.2$, as determined by gel-permeation chromatography in THF, calibrated against PI standards.

High-resolution ^1H and ^{13}C NMR spectra were recorded on a Bruker DPX-400 spectrometer. All imaging experiments were performed on a Bruker DSX-400 spectrometer operating at 9.4 T (400 MHz proton resonance frequency) equipped with a double resonance microimaging probe of 2.3 cm diameter and actively shielded gradient coils. The polymer samples containing ^{13}C -enriched PI were positioned directly in a plexiglass holder inserted in the probehead and centered in the coil. It was found that the small axis of the two-dimensional samples should be perpendicular to the B_0 field of the magnet in order to achieve a satisfactory z -shimming.

The cyclic cross-polarization spin-echo imaging sequence for indirectly detected ^{13}C imaging is constituted of two modules, an editing and an imaging part (Figure 1). The editing part consists of a forward $^1\text{H} \rightarrow ^{13}\text{C}$ and a reverse $^{13}\text{C} \rightarrow ^1\text{H}$ polarization transfer sequence. The (rf) radio frequency SL and CP pulse strengths are adjusted to satisfy the Hartmann–Hahn condition³⁶

$$\gamma_C B_{\text{eff},C} = \gamma_H B_{\text{eff},H} \quad (1)$$

for a selected CH_N molecular group. This is done by an appropriate choice of the experimental parameters. Specifically, the irradiation frequencies for the proton and carbon channel are set on-resonance with respect to the resonances

of the nucleus of the selected molecular group. Furthermore, SL and CP times t are set nominally to

$$t = \begin{cases} J^{-1} & (\text{CH group}) \\ (\sqrt{2}J)^{-1} & (\text{CH}_2 \text{ group}) \\ \approx 0.61 J^{-1} & (\text{CH}_3 \text{ group}) \end{cases} \quad (2)$$

Between the forward and the reverse transfer periods, the ^{13}C coherence is stored as longitudinal magnetization. This intermediate interval serves for the "saturation" of all non-coupled protons. In our study of elastomers, the ratio of T_2^*/T_1 is sufficiently small and therefore a short waiting period on the order of T_2^* is sufficient to destroy all noncoupled proton coherences.

After the backward cross-polarization step, $^{13}\text{C} \rightarrow ^1\text{H}$, the resulting NMR signal arises solely from protons that are coupled to the ^{13}C nucleus of the selected molecular group. It can be used either for spectroscopy or, in combination with a standard NMR spin-echo imaging sequence,³⁶ to reveal the desired spatially resolved information about the distribution of the selected molecular group within the sample.

It should be kept in mind that, in CYCLCROP ^{13}C imaging, one is a priori interested in creating true ^{13}C spin density maps that reflect the quantitative distribution of the selected hydrocarbon molecule within the sample. In elastomers, however, different signal attenuating relaxation mechanisms can play an important role. In this case, measures for the compensation of relaxation losses weighting the signals must be considered.

Figure 1b shows some experimental details of the two different cross-polarization schemes used in this study. The first technique used was the MOIST sequence as suggested in ref 24, involving soft rf pulses of total duration t_{CP} on both channels with Hartmann/Hahn mismatch effects³³ minimized by periodic simultaneous phase shifts of 180° . In the following, we shall refer to this J cross-polarization transfer method as MOIST.

The second method used was the pulsed rotating frame transfer sequence with windows (PRAWN), which employs a comb of m short pulses of duration τ_1 separated by a delay τ_2 .³⁴ The total cross-polarization duration for PRAWN is given by $t_{\text{CP}} = m(\tau_1 + \tau_2)$. The ratio $\tau_1/(\tau_1 + \tau_2)$ is the duty cycle. Since during cross-polarization rf irradiation is applied on both channels even a moderate reduction of the duty cycle below 1 requires significantly less rf power on average.

Results and Discussion

CYCLCROP Imaging with Natural Abundance PI. Figure 2a presents the ^1H NMR spectrum of a sample consisting of two different pieces of polymer, a piece of commercial na-PI next to a piece of common laboratory rubber hose. This spectrum consists of two peaks, the one at high-frequency coming from the methine CH carbon of PI, while the rest of the PI protons and the rubber hose protons give rise to the broad peak at low frequency. The ^1H spectrum of Figure 2b was obtained with the MOIST variant of the CYCLCROP sequence with the proton and carbon channels centered at the respective resonance frequencies of the CH group of PI. It can be seen that all proton coherences not coupled to the PI methine carbon have been successfully edited out, including the protons of the rubber hose.

The next step is to apply the CYCLCROP sequence in combination with a field gradient in order to obtain encoding of the ^1H signal in one space dimension. Parts c and d of Figure 2 display the ^1H NMR profiles of the same sample along the x axis of the laboratory frame. The unedited ^1H profile (Figure 2c) displays both polymer pieces, with the intensity of the rubber protons being much larger than that of PI. In the CYCLCROP

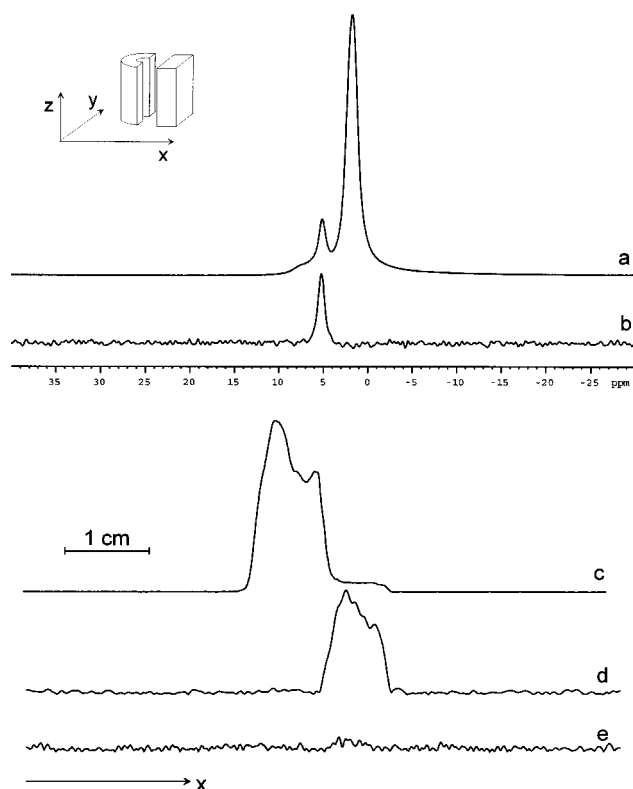


Figure 2. (a) ^1H NMR spectrum of a polymer sample consisting of natural abundance PI and a piece cut from a laboratory rubber hose. (b) CYCLCROP ^1H spectrum of the same sample tuned to the frequency of the methine C-3 group of PI; eight transients. (c) Conventional ^1H NMR profile along the x axis of the same sample. (d) CYCLCROP profile along the x axis tuned to the frequencies of the methine C-3 group of PI. (e) Same as (d) but with the contact pulses on the ^{13}C side set to zero power.

profile (Figure 2d) only the CH PI protons contribute to the signal, so that the rubber hose has been completely edited out. This leads to a profile where only the PI piece appears.

The fact that the signal seen in the CYCLCROP profile comes from the methine PI proton coherence can be verified by the profile in Figure 2e, which was obtained with the CYCLCROP pulse sequence, but with the ^{13}C contact pulses power level set to zero. No intensity can be seen in this profile, as expected if the coherence pathway actually observed in the CYCLCROP profile goes through the methine carbon.

Figure 3 presents the ^1H NMR images obtained for the same sample with normal proton acquisition and with CYCLCROP, respectively. The ^1H image displays both pieces of the polymer sample, while in the CYCLCROP image only the PI piece is visible. No slice selection was applied, and the sample was ~ 1 cm long in the direction perpendicular to the image plane. The CYCLCROP image was acquired in just 43 min and demonstrates the power of proton-detected ^{13}C imaging in creating molecule selective contrast.

CYCLCROP Imaging of ^{13}C -Enriched PI/PB. The imaging experiments presented so far showed that cyclic J cross-polarization can be used as an efficient editing tool for the recording of ^1H NMR images of a specific elastomer in a composite sample. For polymer objects in the range of a few grams the use of natural abundance samples can be afforded without resulting in extremely long image acquisition times. However, in

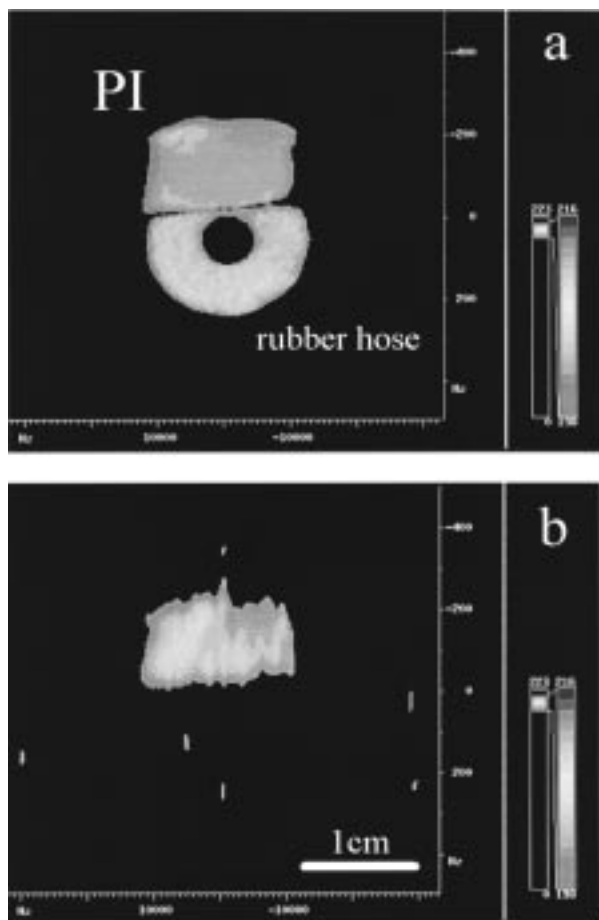


Figure 3. ¹H NMR images of the PI/rubber hose sample. (a) Conventional ¹H NMR image showing both polymer pieces. Parameter values: FOV 4 × 4 cm²; read gradient 41 mT/m; phase gradient 44 mT/m; $T_R = 0.5$ s; $T_E = 2.4$ ms; pixel matrix 256 × 128 zero-filled to 256 × 256. (b) CYCLCROP image of the same sample with the imaging pulse sequence of Figure 1 tuned to the frequencies of the methine C-3 group of PI, where the proton signal from the rubber hose has been eliminated. Parameter values: FOV 4 × 4 cm²; read gradient 41 mT/m; phase gradient 11 mT/m; $T_R = 0.6$ s; $T_E = 2.4$ ms; pixel matrix 256 × 32 zero-filled to 256 × 256; 128 transients; experiment time 43 min.

many cases of interest the polymer sample size has to be much smaller, in the range of tens of milligrams for example. In this case, and due to the low natural abundance of the ¹³C isotope, the use of non-¹³C-enriched polymers is not efficient and actually restricts the range of experimental NMR approaches that can be utilized. For the purpose of exploring the use of CYCLCROP imaging with elastomers in more detail and with smaller sample sizes, polyisoprene 50% enriched in ¹³C at the methylene C-4 position was synthesized in the laboratory.

The ¹H and ¹³C high-resolution spectra of ¹³C-PI in CDCl₃ solution are presented in Figure 4. A polymer sample was constructed by mixing 43 mg of ¹³C-PI with 31 mg of PB in a plexiglass holder, heating for ~3 h at 60 °C in an oven, and cooling for a period of several weeks at room temperature. This procedure resulted in the preparation of a polymer mixture containing 58% w/w ¹³C-PI and consisting of regions possessing an excess of either ¹³C-PI or PB. A quantity of pure ¹³C-PI and PB was put at the higher left and right, respectively, of the plexiglass sample holder to serve as an external reference.

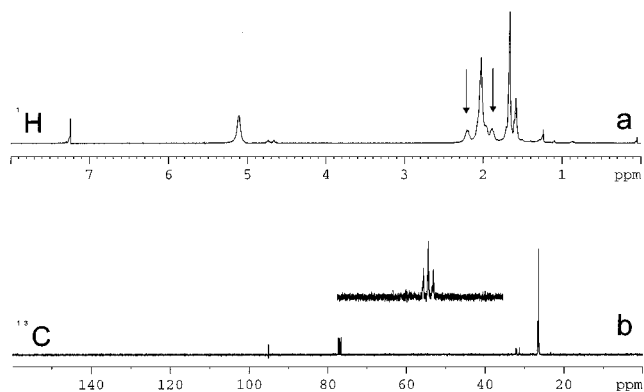


Figure 4. High-resolution NMR spectra of PI¹³C-enriched at the C-4 methylene position, in CDCl₃. (a) ¹H spectrum. Arrows indicate the methylene doublet due to *J*-coupling with ¹³C-4. (b) ¹³C spectrum, ¹H-decoupled. The insert is the coupled spectrum of the methylene peak at ~28 ppm.

Figure 5a presents the ¹H image of the PI/PB sample. A rather homogeneous distribution of proton intensity throughout the sample is observed. Both PI and PB external references can be seen in the proton image of Figure 5a. The 1D proton spectrum of the PI/PB sample is similar to that of Figure 2a, with the methine protons of PI and PB contributing to the high-frequency peak, while the rest of the protons give rise to a low-frequency broad peak of 700 Hz (FWHH).

A problem one has to face at this point when trying to apply CYCLCROP in such a sample is the accurate setting of the ¹H frequency exactly on resonance with the desired proton peak, when this peak is positioned in a broad and featureless line consisting of many types of magnetically inequivalent protons. This problem was not present with the na-PI CYCLCROP imaging experiments, since the methine proton peak was well resolved. In the ¹³C-PI/PB sample, however, one has to locate the exact frequency of the H-4 methylene protons inside the low-frequency unresolved broad peak also containing the H-1 and H-5 protons from PI and the methylene protons of PB.

We found that, guided by the high-resolution ¹H and ¹³C spectra of ¹³C-PI and using the high-frequency ¹H methine peak as an approximate chemical shift reference, it was easy to locate the exact position of the protons attached to the C-4 PI carbon in the broad low-frequency proton peak (see Figure 2a). Exact optimization of the ¹H frequency could then easily be done by means of the CYCLCROP sequence itself. The CYCLCROP image of the ¹³C-PI/PB mixture, with the ¹H and ¹³C channel frequencies centered on the ¹³CH₂ moiety of PI is presented in Figure 5b. The ¹³C-PI reference can still be seen in the upper left of the image, while the PB reference at the upper right produces no intensity at all. Thus it can be concluded that the CYCLCROP image of the polymer mixture represents the spatial distribution of PI in this sample.

With the help of the PI and PB references, difference images can be produced by subtracting the CYCLCROP image of Figure 5b from the normal proton image. The resulting semiquantitative difference ¹H image is displayed in Figure 5c and represents the spatial distribution of PB in the polymer mixture, as can be easily verified by the appearance of the PB reference in the upper right. The ring structure visible in the ¹H image of Figure 5a is not visible in the CYCLCROP image, thus it is coming from PB. However, since it is of low

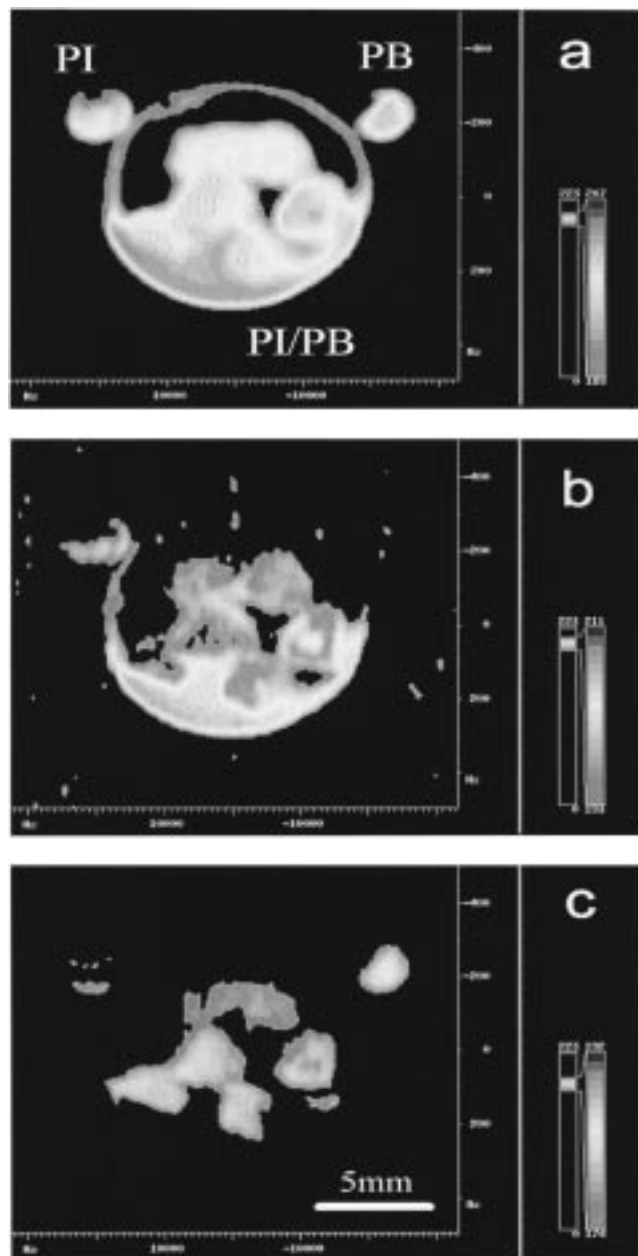


Figure 5. ^1H NMR images of the ^{13}C -PI/PB sample, no slice selection, sample thickness ~ 1 mm. (a) Conventional ^1H NMR image showing the PI and PB references and the ^{13}C -PI/PB mixture. Parameter values: FOV 2×2 cm 2 ; read gradient 81 mT/m; phase gradient 43 mT/m; $T_R = 0.5$ s; $T_E = 2.4$ ms; pixel matrix 256×64 zero-filled to 256×256 . (b) CYCLCROP image of the same sample with the imaging pulse sequence of Figure 1 tuned to the frequencies of the methylene C-4 group of PI and displaying the spatial distribution of PI in the polymer mixture. The PB reference is no longer visible. Same parameter values as in (a), but 1k transients; experiment time 7.5 h. (c) Difference image (a) - (b) normalized to minimum intensity at the PI reference (top left). Qualitative information regarding the distribution of PB in the polymer mixture is obtained from this image.

intensity, it cannot be seen in the difference image of Figure 5c unless a much larger vertical intensity scale is used for the image display (not shown).

The signal-to-noise ratio (S/N) of the CYCLCROP image of Figure 5b was not as high as expected from theoretical treatments of the cross-polarization dynamics in AX_n J -coupled spin systems. For this reason a directly detected ^{13}C image of the ^{13}C -PI/PB sample was recorded, with the purpose of comparing it with CY-

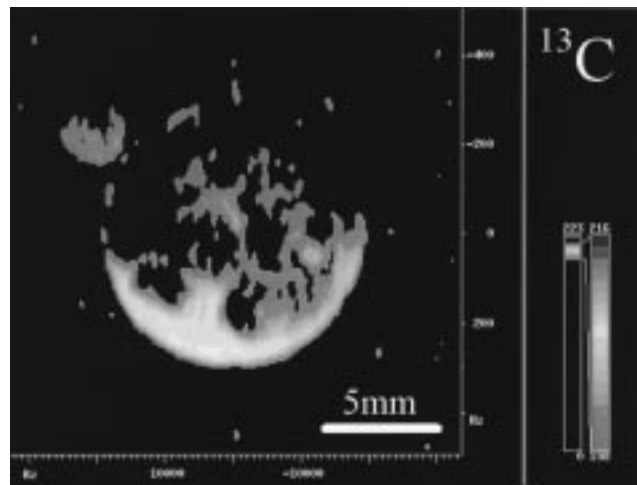


Figure 6. Conventional one-pulse ^{13}C image of the ^{13}C -PI/PB sample, using the same pulse sequence as in Figure 5a. Parameter values: FOV 2×2 cm 2 ; read gradient 328 mT/m; phase gradient 173 mT/m; $T_R = 0.46$ s; $T_E = 2.5$ ms; pixel matrix 256×64 zero-filled to 256×256 ; 2k transients; experiment time 17 h.

CLCROP and assessing the advantages of using cross-polarization for imaging such samples. The ^{13}C image of the ^{13}C -PI/PB sample is presented in Figure 6. Its appearance is similar to that of the CYCLCROP image, thus proving that the latter also produces ^{13}C -edited ^1H images of the spatial distribution of a particular proton coupled to a ^{13}C nucleus. An approximate S/N ratio was calculated for the two images by dividing the integral of the region of the image containing PI/PB with that of a region of pure noise. The calculated S/N ratio of the ^{13}C image of Figure 6 was about half that of the CYCLCROP image of Figure 5a, although the acquisition of the directly detected ^{13}C image took twice as long. Thus, under identical experimental conditions and for the same number of transients, an overall signal enhancement of 2.8 over the direct ^{13}C image is obtained by using the CYCLCROP imaging sequence. This enhancement is lower than that expected in ideal conditions of long relaxation times; for example, compared to an NOE-enhanced directly detected ^{13}C image, CYCLCROP is expected to give an S/N enhancement of $1/3 \cdot (\delta_{\text{H}}/\delta_{\text{C}})^{5/2} = 10.6$. The enhancement of 2.8 is nevertheless very significant in terms of experimental time savings, since the time needed to acquire a ^{13}C -edited CYCLCROP image is still $1/8$ th of that needed for a directly detected ^{13}C image of the same S/N.

Comparison of PRAWN vs MOIST Cross-Polarization. The rf power deposition in the sample during cross-polarization pulses was examined in ref 30. Even at the high frequencies of our present experiments, thermal effects can be excluded. This applies all the more with the nonaqueous samples used in this study. The reduction of the average rf power deposition by the PRAWN sequence therefore is not the main motivation for trying this alternative cross-polarization scheme. On the other hand, any variant of the CYCLCROP preparation sequence may change the selectivity properties of the imaging procedure. In the following we compare results obtained with the aid of the two modifications considered in this context.

Figure 7 presents the CYCLCROP spectra of PI in CDCl_3 solution and in the bulk using both MOIST and PRAWN methods for effecting cross-polarization. Spectra a and b in Figure 7 reveal that both methods behave

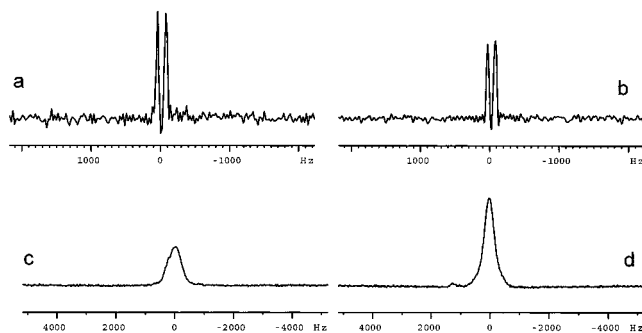


Figure 7. ^{13}C -edited ^1H spectra for the cyclic $^1\text{H} \rightarrow ^{13}\text{C} \rightarrow ^1\text{H}$ polarization transfer in the rotating frame for the methylene C-4 group of ^{13}C -PI in CDCl_3 solution (a, b) and in bulk ^{13}C -PI/PB (c, d) using MOIST (right) and PRAWN (left) variants for effecting J cross-polarization.

similarly in solution, in accordance with recent results of a CYCLCROP application in imaging of plants.³¹ The duty cycle used for PRAWN with the PI solution was only 0.2, where B_1 fields of ca. 0.8 kHz amplitude were used as in the case of the MOIST variant. However, in the case of bulk PI in the PI/PB sample the efficiency of the two techniques was not the same, as is clearly seen in spectra c and d of Figure 7. Integration of the CYCLCROP proton peaks showed that only 55% of the signal is acquired with PRAWN compared to MOIST.

Figure 8 shows the CYCLCROP images of a blend of ^{13}C -PI and poly(hydroxyoctanoate), PHO, produced by melting the two elastomers together in a plexiglass holder and cooling for several weeks at room temperature. Although both PRAWN and MOIST are efficient in editing out the PHO reference visible on the higher left of the ^1H image, the S/N ratio of the image acquired with PRAWN is about 65% of that of the image acquired with MOIST. A duty cycle of 0.5 was used for PRAWN in the imaging of the PI/PHO blend. Since both methods were equivalent in solution, it appears that the reduced S/N ratio of the bulk images is a result of the different rotating frame relaxation properties and the heterogeneity of elastomers in the bulk phase compared to solution, given that the average rf field over the mixing time differed by a factor of 2 in the two cases. It is well-known that the short T_2 in bulk elastomers is responsible for their large line widths compared to polymer solutions.

Also, bulk magnetic susceptibility and spin diffusion are factors that become important in the solid state and affect $T_{\rho,\text{eff}}$.³⁷ Since with PRAWN rf irradiation is not "on" continuously, it is possible that semirigid or inter-phase regions close to crystallites, where spin diffusion is more effective are less likely to be efficiently cross-polarized. This means that the reduced intensity and the somewhat different contrast obtained in the PRAWN image of the PI/PHO blend in Figure 8 could be related to the absence of contribution to the signal intensity of regions of lower mobility. Thus an additional relaxation contrast might be afforded with CYCLCROP depending on the method used to effect the cyclic polarization transfer. This aspect appears to warrant closer investigation, including the behavior with the refocused PRAWN- π sequence.³⁴

Factors Affecting Cross-Polarization Efficiency in Elastomers. During the course of the NMR imaging experiments using cross-polarization as an editing tool, some interesting features regarding the behavior of the CYCLCROP imaging pulse sequence were noted. These

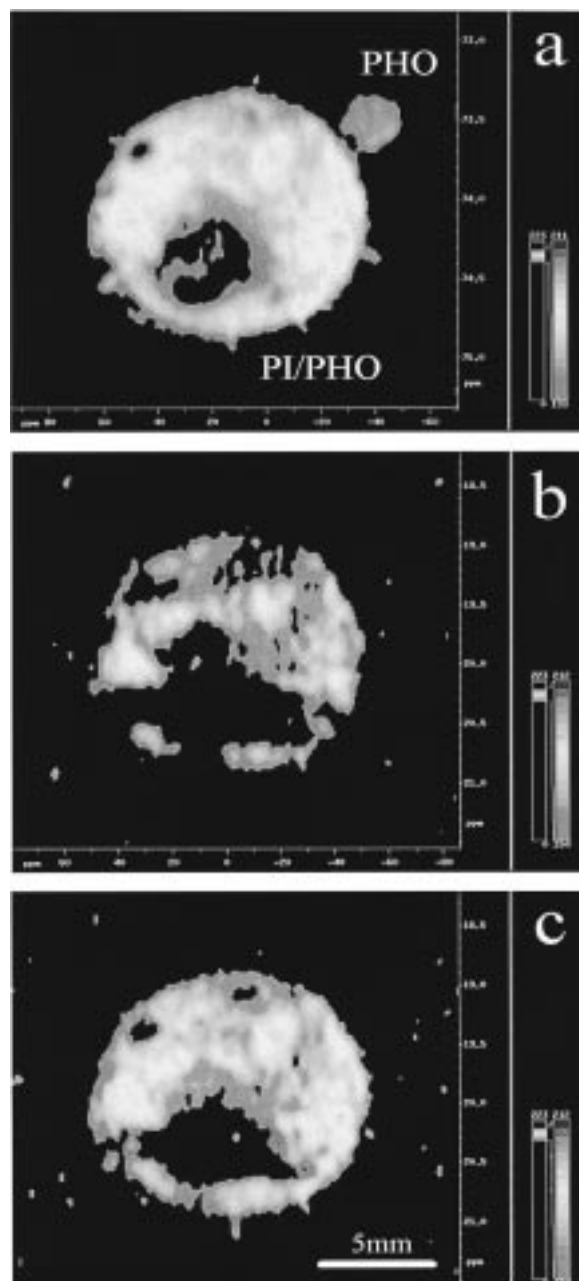


Figure 8. ^1H NMR images of a ^{13}C -PI/PHO blend, no slice selection, sample thickness ~ 1 mm. (a) Conventional ^1H NMR image showing the PHO reference (top left) and the ^{13}C -PI/PHO mixture. Parameter values: FOV 2×2 cm 2 ; read gradient 81 mT/m; phase gradient 43 mT/m; $T_R = 0.5$ s; $T_E = 2.4$ ms; pixel matrix 256×64 zero-filled to 256×256 . (b), (c) CYCLCROP image of the same sample with the imaging pulse sequence of Figure 1 tuned to the frequencies of the methylene C-4 group of PI, using PRAWN (b) and MOIST (c) and displaying the spatial distribution of PI in the polymer blend. The PHO reference is no longer visible. Same parameter values as in (a), experiment time 7.5 h.

were attributed to the special spin properties of the samples used, namely bulk elastomeric materials, with respect to previous experiments performed with liquids. The value of the optimum cross-polarization time for the transfer of magnetization depends on the coupling between the two spins and, for a CH_2 group, without taking into account any relaxation effects, is given by eq 2 to $(J\sqrt{2})^{-1}$ where J is the effective coupling constant.

However, in imaging experiments using the cyclic cross-polarization pulse sequence of Figure 1, such as those presented in Figure 5, the optimum cross-polarization time was found to vary between 3.7 ms for MOIST and 4.5 ms for PRAWN. The value calculated from the coupling constant value $J = 127$ Hz in the methylene group of C-4 in PI is 5.6 ms. There are two possible reasons that could be responsible for the shorter optimum mixing time observed. The first involves the possible contribution of the residual dipolar coupling between the two spins, which acts to increase the effective coupling during the cross-polarization interval (see ref 36, p 360). In this case J should be replaced with the total effective coupling summed over all coupling mechanisms present. Motional averaging in elastomers succeeds in removing most of the dipolar interaction; however, as suggested by the large line widths of both ^1H and ^{13}C spectra of bulk PI, 700 and 70 Hz, respectively, some residual broadening still remains.³⁷

The second reason for obtaining a short time maximum for the optimum contact pulse duration is the effect of short relaxation time in the rotating frame, $T_{\rho,\text{eff}}$. In this case, the oscillation of magnetization between the two spins during cross-polarization is damped by short $T_{\rho,\text{eff}}$ values, resulting in asymmetric curves for the coherence transfer function, having a maximum at shorter than ideally predicted mixing times.³⁸ Very short $T_{\rho,\text{eff}}$ values would additionally explain the reduced enhancement (~ 3) obtained in the CYCLCROP images compared to the theoretical maximum of 10 for a CH_2 spin system. Note that during cross-polarization both the ^1H and the ^{13}C nuclei are involved in the relaxation process, so one refers to an "effective" relaxation time $T_{\rho,\text{eff}}$ in the rotating frame for the whole molecular $^{13}\text{CH}_N$ group.³¹

A number of 2D NMR experiments investigating the cross-polarization dynamics in elastomeric materials were designed in order to clarify their behavior during the CYCLCROP imaging experiments already reported. In these experiments the coherence transfer (CT) function during the cross-polarization mixing time was studied. The second dimension, f_1 , was introduced by stepping the duration of the cross-polarization mixing time, while the first dimension was the usual ^{13}C or ^1H spectroscopic dimension. By Fourier transformation, the coherence transfer spectrum can be obtained, and from it one can easily extract the frequency of the coherence transfer, and the $T_{\rho,\text{eff}}$ responsible for relaxation during the cross-polarization interval. The 2D CT experiment was performed for the forward ($^1\text{H} \rightarrow ^{13}\text{C}$), the reverse ($^{13}\text{C} \rightarrow ^1\text{H}$), and the cyclic polarization transfer ($^1\text{H} \rightarrow ^{13}\text{C} \rightarrow ^1\text{H}$).

The coherence transfer was studied with both variants of the CYCLCROP pulse sequence, MOIST and PRAWN, and using both the PI/PB sample of the images of Figure 5 and a second sample that consisted of a CDCl_3 solution of ^{13}C -PI. The solution sample was used as a reference because of the absence of any residual dipolar interactions in the liquid state. Figure 9 presents the 1D projection (along f_1) of the 2D coherence transfer spectra obtained for the cyclic polarization transfer ($^1\text{H} \rightarrow ^{13}\text{C} \rightarrow ^1\text{H}$) in the ^{13}C -PI solution (a, b) and the bulk PI/PB sample (c, d), with both MOIST (right) and PRAWN (left) sequences. These projections, which are approximately symmetric around the central peak, represent the CT frequencies in the

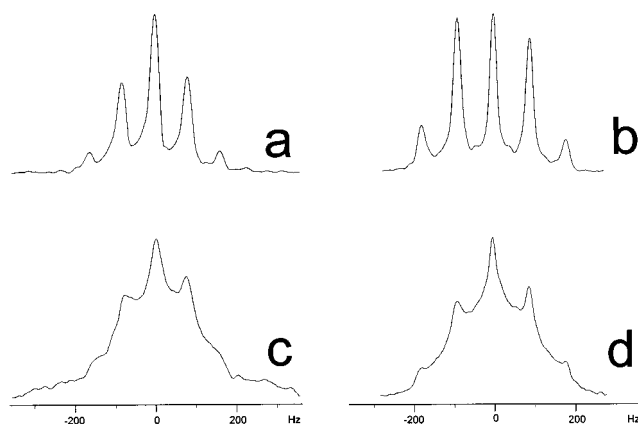


Figure 9. (a) Projection of the 2D coherence transfer spectra on the f_1 dimension for cyclic $^1\text{H} \rightarrow ^{13}\text{C} \rightarrow ^1\text{H}$ rotating frame polarization transfer of the C-4 methylene group of ^{13}C -PI in CDCl_3 solution (a, b) and in bulk PI/PB (c, d) using the PRAWN (left) and MOIST (right) variants of J cross-polarization.

rotating frame, according to the equation:³⁴

$$f_{\text{CT}}(2t) \sim \left(\frac{3}{2} - 2 \cos \sqrt{2}\pi Jt + \frac{1}{2} \cos 2\sqrt{2}\pi Jt \right) \exp(-t/T_{\rho,\text{eff}}^f) \exp(-t/T_{\rho,\text{eff}}^r) \quad (3)$$

where the upper indices in the rotating frame relaxation times stand for forward, f, and reverse, r, polarization transfer. Equation 3 holds when all proton coherences other than that of the cross-polarization pair are successfully dephased in the interval between the two polarization transfers, either by spoiling gradients,²⁴ or by introducing a time delay, as in the present case. The peaks in Figure 9 are situated at the coherence transfer frequencies $\nu_1 = \pm J/\sqrt{2}$ and $\nu_2 = \pm 2J/\sqrt{2}$ according to eq 3, and their line widths depend on $T_{\rho,\text{eff}}$ according to $\text{FWHM} = \sqrt{3}/\pi T_{\rho,\text{eff}}$, where $T_{\rho,\text{eff}}^{-1} = T_{\rho,\text{eff}}^f{}^{-1} + T_{\rho,\text{eff}}^r{}^{-1}$. The factor $\sqrt{3}$ takes into account the magnitude mode of the 2D spectra.

The CT projections of PI in bulk are clearly much broader than in solution. Thus it appears that the effective relaxation time in the rotating frame is much longer in solution than in bulk. To calculate the FWHM for the five peaks of the bulk PI f_1 projections, these were deconvoluted with Lorentzian line shapes. The $f_{\text{CT}}(2t)$ and $T_{\rho,\text{eff}}$ data extracted from the CT spectra of Figure 9 for the cyclic polarization transfer case, along with those extracted from similar experiments for the single forward and reverse case, are collected in Table 1. The coherence transfer frequency does not differ within experimental error in solution (~ 90 Hz) and in bulk (~ 85 Hz), although it is on average slightly lower in the bulk. The frequency value expected from the J -coupling of 127 Hz in the methylene group of PI is 89 Hz. These data then are evidence that no other **discrete** coupling is involved during the oscillatory cross-polarization in bulk PI. The $T_{\rho,\text{eff}}$, however, is significantly larger in solution than in bulk. For the forward polarization transfer $T_{\rho,\text{eff}}$ is 5 times smaller in the bulk, while for the reverse and cyclic cases it is about 2 times smaller. When the $T_{\rho,\text{eff}}$ is known, one can calculate the theoretical optimum (one-way) cross-polarization time for a CH_2 spin system by the equation³¹

$$t_{\text{opt}} = \frac{\sqrt{2}}{\pi J} \tan^{-1}(\sqrt{2}\pi J T_{\rho,\text{eff}}) \quad (4)$$

Table 1. Coherence Transfer Frequency, ν_1 (Hz), and Effective Relaxation Time in the Rotating Frame, $T_{\rho, \text{eff}}$ (ms), during Polarization Transfer in the Methylene C-4 Group of PI, in Solution and in Bulk

	$^1\text{H} \rightarrow ^{13}\text{C}$				$^{13}\text{C} \rightarrow ^1\text{H}$				$^1\text{H} \rightarrow ^{13}\text{C} \rightarrow ^1\text{H}$			
	ν_1		$T_{\rho, \text{eff}}^f$		ν_1		$T_{\rho, \text{eff}}^f$		ν_1, ν_2		$T_{\rho, \text{eff}}$	
	PRAWN	MOIST ^b	central	outer	PRAWN	MOIST	central	outer	PRAWN	MOIST	central	outer
PI in solution	91	92	50	42	90	88	18	16	91 181	89 178	18	15
PI/PB bulk	83	82	7	10	84	88	6	8	84 170	86 173	8	8

^a In MOIST, phase alternation (x, -x) was performed every 925 μs . ^b Phase alternation (x, -x) every 615.4 μs .

With the $T_{\rho, \text{eff}}$ values from Table 1, the optimum cross-polarization times for the C-4 methylene group of bulk PI with the MOIST and PRAWN sequences is calculated as 4.7 ms. This value is in good agreement with the value of 4.5 ms determined experimentally for PRAWN, although it is still somewhat larger than the value of 3.7 ms determined for MOIST under conditions of cyclic cross-polarization.

Equation 3 predicts that the relaxation behavior during a cyclic cross-polarization will be guided by the shorter $T_{\rho, \text{eff}}$ value of either the forward or the reverse transfer. In the case of the 2D CT experiments performed for PI in bulk, both single transfers have equally small $T_{\rho, \text{eff}}$ values; thus this effect is not readily recognized. However, the results obtained for PI in solution and presented in Table 1 demonstrate this point convincingly for both MOIST and PRAWN, since the $T_{\rho, \text{eff}}$ of the cyclic cross-polarization is found to be the same as that of the reverse transfer, although the forward transfer has a 5 times larger value.

Another interesting trend observed in Table 1 is that the $T_{\rho, \text{eff}}$ of the central peak of the CT spectra of PI in both solution and bulk is bigger for MOIST than for PRAWN for both the forward and the reverse polarization transfer cases. In the cyclic transfer this effect is suppressed by the dominance of the shorter $T_{\rho, \text{eff}}$ with both cross-polarization methods. This difference in $T_{\rho, \text{eff}}$ reflects the fact that in MOIST the spin-lock condition is more effective because of the continuous application of phase-alternated rf fields on both channels during cross-polarization, while with PRAWN, irradiation is discontinued at regular intervals: in these experiments the average rf field of MOIST has twice the amplitude of that of PRAWN. In the case of the bulk PI/PB sample, where spin diffusion is very effective, ^1H nuclei that lose the spin-lock condition during the τ_2 delay in PRAWN will be quickly dephased through spin diffusion and will not contribute to the signal, leading to a reduction of S/N ratio.

This is exactly what has been observed in the CYCLCROP images of Figure 8, where it was shown that the number of spins undergoing cross-polarization is smaller with PRAWN than with MOIST. Since spin diffusion is more effective in less mobile (more rigid) regions, this observation lends support to the hypothesis that the observed differences in contrast in Figure 8 could relate to the different behaviors of the two mixing sequences vis-à-vis degrees of mobility in different regions of the sample.

Conclusions

The primary goal of this study was not to produce any relaxation-related contrast in the images. We rather focused on mapping the ^{13}C spin density selectively for different chemical groups. This is an objective entirely different from ordinary magnetic resonance imaging where contrast represents the combined effect of different material and experimental parameters.

Due to the wide chemical-shift range of ^{13}C , the CYCLCROP imaging pulse sequence forms a particularly suitable technique for the study of heterogeneous elastomeric materials, or rigid materials containing one or more elastomeric parts. The ability to provide spatial maps of the distribution of one polymer component in a heterogeneous polymer matrix is of prime importance, since the contrast obtained is much better than the relaxation contrast, which requires medium to large

differences in relaxation between components in order to be effective.

With respect to sensitivity enhancement, although due to short relaxation times in the rotating frame the full potential of the polarization transfer is not exploited, still an at least 8-fold reduction in experiment duration was obtained with CYCLCROP using MOIST, with respect to direct one-pulse ^{13}C imaging. This advantage stems from performing the initial excitation and the detection on the proton channel. Thus CYCLCROP combines the high sensitivity of ^1H imaging with the 10 times wider chemical shift range available for editing on the carbon side. Possible applications include imaging of the distribution of elastomeric components in composite materials, the diffusion of solvents in elastomers, or very slow diffusion of elastomers in a polymer matrix. The sensitivity of the technique is sufficient to allow experiments with natural abundance industrial samples of moderate size, as has been demonstrated in this publication. More advanced applications could benefit from ^{13}C -enriched materials, depending on the design of the imaging experiment.

It is interesting to note that, contrary to expectations, the lack of resolution in the ^1H spectrum of the polymers studied did not present any obstacle for performing the cyclic polarization transfer. For example, the image of Figure 5b uses the C-4 methylene pair of PI for the cross-polarization, whose methylene protons are buried in a 700 Hz wide peak containing four different proton species from two different polymers. The approximate position of the ^1H peak of interest can be estimated from high-resolution solution spectra, and its exact position can be optimized for maximum signal intensity with the 1D variant CYCLCROP sequence itself.

Thus CYCLCROP allows proton-detected ^{13}C imaging of completely unresolved proton peaks. The distinction of different polymers in blends is possible as far as the ^{13}C resonances of specific hydrocarbon groups can be resolved. As the chemical shift range of ^{13}C is about 10 times wider than that of protons, it is obvious that indirectly detected ^{13}C imaging is superior to direct ^1H spin density mapping. With respect to emulsions and blends of different tacticities, for instance, the CYCLCROP imaging method promises selective access to the different species even when proton resonances are no longer resolved.

From the experimental work presented here, it can be concluded that the PRAWN and MOIST cross-polarization variants used in this study have similar efficiencies for elastomers in solution. In the imaging of bulk elastomer samples, the efficiency of PRAWN—for a fixed peak rf field amplitude—seems to be reduced by the effect of spin diffusion. However, this opens up the possibility of using CYCLCROP to obtain images that possess a “two-level” editing. On the first level, cyclic cross-polarization is used to image exclusively the desired molecular species, leading to edited images of a single component of a composite material. Furthermore, a second level of contrast in the proton-detected ^{13}C images can be achieved by using PRAWN, its refocused variant, or MOIST to effect cross-polarization. PRAWN proves convenient in effecting cross-polarization efficiently in polymer solutions with average B_1 fields of the order of the coupling constant. While both sequences are clearly well suited for indirectly detected ^{13}C imaging of elastomers in the “solid state”, it seems worthwhile to explore further the preliminary evidence presented here in regard to the possible mobility

contrast characteristics of the two sequences.

Acknowledgment. We thank Dr. U. Görke, H. Wiringer, and K. Gille for assistance in the course of this work. A.S. is indebted to the Alexander von Humboldt Foundation for a research fellowship (GRI 102 7150). Financial support by the Deutsche Forschungsgemeinschaft is also acknowledged.

References and Notes

- (1) Wehrli, F. W.; Shaw, D.; Kneeland, J. B., Eds. *Biomedical Magnetic Resonance Imaging: Principles, Methodology and Applications*; VCH Publishers: New York, 1988.
- (2) Blümich, B.; Kuhn, W., Eds. *Magnetic Resonance Microscopy*; Verlag Chemie: Weinheim, 1992.
- (3) Hafner, S.; Demco, D. E.; Kimmich, R. *Solid State NMR* **1996**, *6*, 275.
- (4) Cory, D. G. *Solid State NMR* **1996**, *6*, 347.
- (5) Scheler, U.; Schauss, G.; Blümich, B.; Spiess, H. W. *Solid State NMR* **1996**, *6*, 375.
- (6) Iwamiya, J. H.; Sinton, S. W. *Solid State NMR* **1996**, *6*, 333.
- (7) Blümmler, P.; Blümich, B. *Macromolecules* **1991**, *24*, 2183.
- (8) Chudek, J. A.; Hunter, G. *J. Mater. Sci. Lett.* **1992**, *11*, 222.
- (9) Hafner, S.; Barth, P. *Magn. Reson. Imaging* **1995**, *5*, 739.
- (10) Spyros, A.; Kimmich, R.; Briese, B. H.; Jendrossek, D. *Macromolecules* **1997**, *30*, 8278.
- (11) Fyfe, C. A.; Randall, L. H.; Burlinson, N. E. *J. Polym. Sci., Part A: Polym. Chem.* **1996**, *31*, 159.
- (12) Hafner, S.; Kuhn, W. *Magn. Reson. Imaging* **1994**, *12*, 1075.
- (13) Sarkar, S.; Komoroski, R. A. *Macromolecules* **1992**, *25*, 1420.
- (14) Garrido, L.; Mark, J. E.; Sun, C. C.; Ackerman, J. L.; Chang, C. *Macromolecules* **1991**, *24*, 4067.
- (15) Smith, S. R.; Koenig, J. L. *Macromolecules* **1991**, *24*, 3496.
- (16) Günther, E.; Blümich, B.; Spiess, H. W. *Macromolecules* **1992**, *25*, 3315.
- (17) Blümich, B. *Acta Polym.* **1993**, *44*, 125.
- (18) Klinkenberg, M.; Blümmler, P.; Blümich, B. *Macromolecules* **1997**, *30*, 1038.
- (19) Miller, J. B.; Garroway, A. N. *J. Magn. Reson.* **1989**, *82*, 529.
- (20) Miller, J. B. *J. Magn. Reson.* **1989**, *85*, 255.
- (21) Szeverenyi, N. M. *J. Magn. Reson.* **1984**, *60*, 460.
- (22) Cory, D. G. *Ann. Rep. NMR* **1992**, *24*, 87.
- (23) Hafner, S.; Demco, D. E.; Kimmich, R. *Chem. Phys. Lett.* **1991**, *187*, 53.
- (24) Kunze, C.; Kimmich, R. *Magn. Reson. Imaging* **1994**, *5*, 805.
- (25) Knüttel, A.; Kimmich, R.; Spohn, K.-H. *J. Magn. Reson.* **1990**, *86*, 526.
- (26) Knüttel, A.; Spohn, K.-H.; Kimmich, R. *J. Magn. Reson.* **1990**, *86*, 542.
- (27) Knüttel, A.; Kimmich, R.; Spohn, K.-H. *Bull. Magn. Reson.* **1990**, *12*, 30.
- (28) Kunze, C.; Kimmich, R.; Demco, D. E. *J. Magn. Reson. A* **1993**, *101*, 277.
- (29) Köstler, H.; Kimmich, R. *J. Magn. Reson. B* **1993**, *102*, 285.
- (30) Kunze, C.; Kimmich, R. *J. Magn. Reson. B* **1994**, *105*, 38.
- (31) Heidenreich, M.; Köckenberger, W.; Kimmich, R.; Chandrakumar, N.; Bowtell, R. *J. Magn. Reson.* in press.
- (32) Kimmich, R.; Görke, U.; Weis, J. *J. Trace Microprobe Techn.* **1995**, *13*, 285.
- (33) Levitt, M. H. *J. Chem. Phys.* **1991**, *94*, 30.
- (34) Chandrakumar, N.; Kimmich, R. Submitted for publication.
- (35) Gajewski, J. J.; Peterson, K. B.; Kagel, J. R.; Jason Huang Y. C. *J. Am. Chem. Soc.* **1989**, *111*, 9078.
- (36) Kimmich, R. *NMR—Tomography, Diffusometry, Relaxometry*; Springer-Verlag: Berlin, Heidelberg, 1997.
- (37) Komoroski, R. A. Carbon-13 NMR of Solid Amorphous Polymers Above T_g . In *High Resolution NMR Spectroscopy of Synthetic Polymers in Bulk*; Komoroski, R. A., Ed.; VCH Publishers Inc.: Deefield Beach, FL, 1986: Chapter 4.
- (38) Chandrakumar, N. Spin-1 NMR. In *NMR Basic Principles and Progress*; Fluck, E., Günther, H., Eds.; Springer-Verlag: Berlin, **1996**; Vol. 34, p 35.